Phonon Focusing Effect in an Atomic Level Triangular Structure

Jian-Hui Jiang(姜剑辉), Shuang Lu(鲁爽), and Jie Chen(陈杰)*

Center for Phononics and Thermal Energy Science, China–EU Joint Lab for Nanophononics, MOE Key Laboratory of Advanced Micro-structured Materials, School of Physics Science and Engineering, Tongji University, Shanghai 200092, China

(Received 25 June 2023; accepted manuscript online 28 July 2023)

The rise of artificial microstructures has made it possible to modulate propagation of various kinds of waves, such as light, sound and heat. Among them, the focusing effect is a modulation function of particular interest. We propose an atomic level triangular structure to realize the phonon focusing effect in single-layer graphene. In the positive incident direction, our phonon wave packet simulation results confirm that multiple features related to the phonon focusing effect can be controlled by adjusting the height of the triangular structure. More interestingly, a completed different focusing pattern and an enhanced energy transmission coefficient are found in the reverse incident direction. The detailed mode conversion physics is discussed based on the Fourier transform analysis on the spatial distribution of the phonon wave packet. Our study provides physical insights to achieving phonon focusing effect by designing atomic level microstructures.

DOI: 10.1088/0256-307X/40/9/096301

Manipulating wave transport by artificial materials is a hot topic in recent years.[1–3] The rapid development of metamaterials has also brought new ideas for designs of acoustic or optical devices with special functionalities, such as beam focusing,[4–7] asymmetric transmission,[8–11] self-bending beams,[12–14] cloak,[15–17] and perfect absorption.[18–20] In addition to modulations of light and sound, there have been growing efforts in applying phononic crystals to control of thermal waves as well,[21–24] namely, the heat.[25–28] Novel structures, such as graded heat-conduction metadevices[29,30] and liquid-solid hybrid thermal metamaterial,[31] have been designed to achieve unusual heat transport behavior.

As a quasi-particle in solids, phonons simultaneously have wave-like and particle-like pictures[32–34] and dominate heat conduction in insulators and semiconductors.[35] The wave-like picture of phonon not only can be used to regulate the thermal transport in materials,[36–38] but also plays an important role in quantum information[39–41] and damage detection.[42,43] Wave focusing plays an important role not only in medical diagnosis and tumor hyperthermia, but also in nondestructive flaw detection techniques in engineering field.[44–46] The focusing of phonon flux in elastically anisotropic solids has been studied to realize quasi-one-dimensional thermal transport in bulk systems,[47–50] which is caused by the fact that the phase and group velocities do not point to the same direction.[47] This kind of phonon focusing is based on the particle-like picture of phonon, which depends critically on the anisotropy of crystals[51–53] but makes no use of the phase control. As the lattice wave has similar properties to acoustic wave, a natural question arises: Is it possible to achieve phonon focusing in isotropic materials by utilizing the phase of lattice waves?

In this Letter, a triangle-shaped atomic level structure is proposed to modulate the propagation of phonon wave packet in graphene. This triangular structure can achieve the phonon focusing effect near the vertex of the triangular structure. By adjusting the height of the triangular structure, multiple features including the position, energy and time of the focusing point can be regulated. More interestingly, different phonon focusing patterns and energy transmission coefficient can be obtained by engineering the phonon incident direction. Our study demonstrates the feasibility of realizing phonon focusing effect via atomic level structure design.

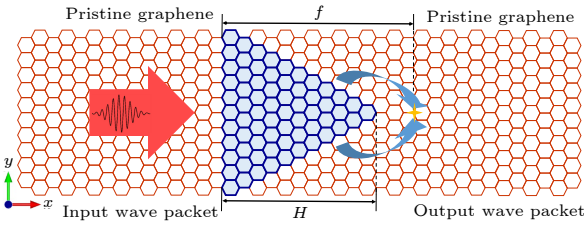

Fig. 1. The schematic graph for the phonon wave-packet simulation in single-layer graphene. The triangular structure is composed of ^{36}C isotope, while the rest part is composed of ^{12}C atom. The height of this triangular structure are labeled as H. A phonon wave packet is launched in the pristine graphene on the left-hand side and transmitted through the structure along the x direction. After the phonon wave packet is transmitted through the structure, the distance from the focusing point and the triangular structure's bottom edge is referred as the focal length f.

Figure 1 shows the schematic graph of the wave-packet simulation. The entire graphene plane is 200 nm long in the x direction and 60 nm wide in the y direction, which are fixed in our simulations. A total of 960000 carbon atoms are used in our simulations, with the atomic mass of 12 g/mol. The C–C bond length is set as $a = 1.44$ Å,

*Corresponding author. Email: jie@tongji.edu.cn
© 2023 Chinese Physical Society and IOP Publishing Ltd

and we set lattice constant $l_0 = \sqrt{3}a$ and inverted vector $q_0 = \frac{2\pi}{l_0}$ for convenience. To build the phonon focusing device, a triangular-shaped atom-scale structure with height $H = 200$ Å and ^{36}C isotopes is constructed (blue region in Fig. 1). We define the focal length f as the distance from focusing point to the base of the triangular structure. Since acoustic phonons make dominant contribution to thermal transport in most crystalline materials, we only consider the propagation of acoustic phonons in our simulation. All wave-packet simulations [54] in this work are performed by using the LAMMPS package [55] with the optimized Tersoff potential [56] for graphene. The timestep is set as 0.5 fs, and periodic boundary conditions are applied in all directions. More details and verification of the accuracy of the method can be found in Section A of the Supplemental Information.

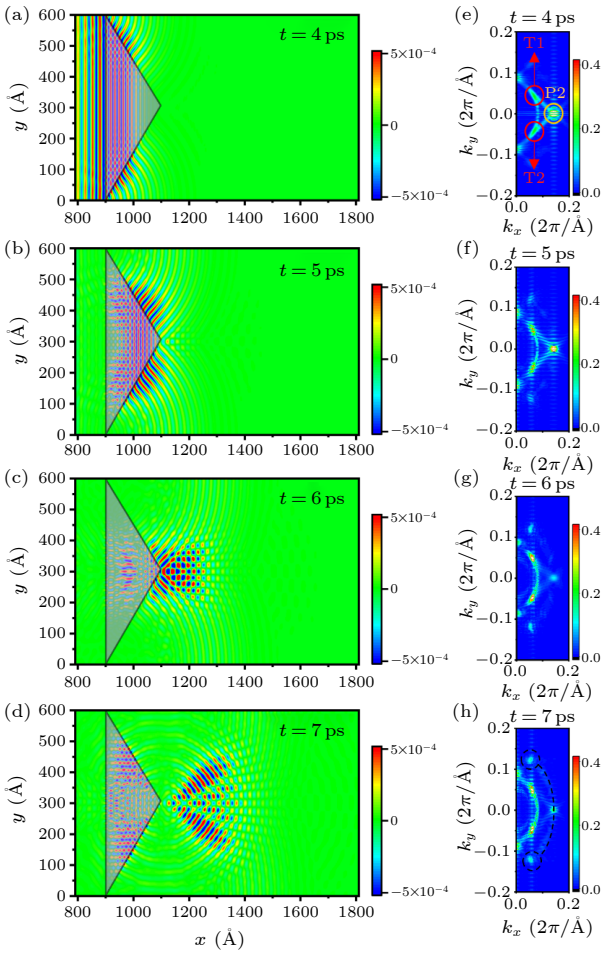

Fig. 2. (a)–(d) Distributions of atomic displacement when the phonon wave packet passes through the triangle-shaped atom-scale structure with $H = 200$ Å at various time snapshots. The bottom edge of the triangular structure is located at $x = 900$ Å and the vertex is located at $x = 1100$ Å. (e)–(h) The corresponding two-dimensional (2D) fast Fourier transform (FFT) of the spatial displacement distribution in a local region ($900\,\text{Å} \leqslant x \leqslant 1600\,\text{Å}$) in (a)–(d), respectively. The colorbar in 2D FFT represents the Fourier transform intensity.

The transverse acoustic (TA) phonon is used as an example to demonstrate the focusing effect in this study. A phonon wave packet is launched on the left pristine graphene segment and propagates toward the graphene plane along the x direction. We observe the waveform in the pristine graphene segment on the right-hand side and analyze their modes.

We first show in Fig. 2 the time evolution of the phonon wave packet passing through the structure. At $t = 4$ ps, the plane wave mostly enters the structure and becomes tilted at two hypotenuses of the triangle [Fig. 2(a)]. After one picosecond of time evolution, these two tilted waves are propagating basically along the direction of the hypotenuse [Fig. 2(b)]. At $t = 6$ ps, two phonon wave packets focus near the vertex of the triangle and generate the interference pattern, as shown in Fig. 2(c). Then two wave packets spread out at $t = 7$ ps [Fig. 2(d)]. The calculation of the energy on both sides reveals that about 42.67% of the incident energy can successfully pass through this structure. The reason for the focusing of phonons is that waves have different phase delays at different vertical positions (y). After passing through the triangular structure, the plane wave will produce a delay in phase, which is proportional to the structure height H. While the local structure height $H(y)$ is a function of y, the plane wave undergoes different phase delays at various y positions, giving rise to the tilted phonon wave packet in real space, as shown in Fig. 2(a) at $t = 4$ ps. In addition to the presence of these two tilted wave packets, there are also series of bending waves connecting the tilted waves to the boundary, which is related to the role of the boundary on the tilted waves. The effect of the periodic boundary on our model is explored in Section B of the Supplemental Information.

To better analyze the time evolution of phonon wave packet, we perform a two-dimensional Fast Fourier transform (2D FFT) of the spatial displacement distribution in a local region ($900\,\text{Å} \leqslant x \leqslant 1600\,\text{Å}$) at various time snapshots. In 2D FFT analysis, the colorbar denotes the Fourier transform intensity. The initial normal incident wave packet at $t = 0$ ps is set as $k_x = 0.08 \times 2\pi\,\text{Å}^{-1}$ and $k_y = 0$, which is denoted as P1 and its 2D FFT is shown in Fig. S1 in the Supplemental Information. Figures 2(e)–2(h) show the corresponding 2D FFT of the spatial distribution in Figs. 2(a)–2(d). At $t = 4$ ps, two new modes with nonzero k_y emerge, marked as T1 and T2 in Fig. 2(e). These two modes have the same k_x but opposite k_y, which means that they are symmetric with respective to the horizontal direction and correspond to the two tilted waves in Fig. 2(a). The horizontal wave packet with $k_y = 0$ shifts to a larger wavevector of $k_x = 0.14 \times 2\pi\,\text{Å}^{-1}$, which is marked as P2 and represents the wave inside the triangular-shaped structure [see Fig. 2(a)]. Due to the larger atomic mass in the triangular structure, the phonon group velocity is reduced compared to the ^{12}C graphene, leading to the increased wavevector of P2 compared to that of P1 as a consequence of elastic process. Similar effect of increased wavevector has also been observed in superlattice structure. [25] As time evolves, more incident energy is influenced by the triangular structure to become tilted waves, so the energy intensities of T1 and T2 become enhanced. Meanwhile, more wave packets have passed through the triangular structure, resulting in the decreased energy of P2.

Moreover, there are also other wave modes in the 2D FFT analysis that deserve attention. As shown in Figs. 2(e)–2(h), series of modes between T1 and T2 emerge, and momentum is conserved among these modes. The mode coupling between T1 (or T2) and P2 represents the series of influences induced by the hypotenuse of the triangle on T1 (or T2). Their intensity rapidly decreases when time evolves to $t = 6$ ps and beyond [Figs. 2(g) and 2(h)]. This is because two tilted wave packets are no longer in contact with the hypotenuse. In addition, two new modes appearing after $t = 4$ ps [dashed circles in Fig. 2(h)] represent two reflected wave modes after the plane wave touches the hypotenuse inside the triangle. It can be seen in Fig. 2(h) that the wavevectors for these mode distribute on the same circle (dashed curve) as the P2 mode, indicating the maintained momentum conservation inside the structure.

The above-stated phenomena indicate that the propagation direction of the lattice wave can be changed by setting the phase difference, which can be used to realize the phonon focusing effect. This has led to our interest in using the triangle-shaped atom-scale structure to regulate the focus of phonon wave packets. To this end, we simulate the propagation of phonon wave packet in various triangular structures with different height H for different phonon wavelengths.

Figure 3 shows the relationship between H and the position of the focal length f for different phonon wavelengths, in which an approximation relation $f \approx H$ can be observed, independent of the phonon wavelength. This means that T1 and T2 modes are always transmitted essentially along two hypotenuses of the triangle structure, and eventually focus near the vertex of the triangle. This feature allows us to regulate the position of the focusing point by changing H. To this end, we choose three representative triangular structures with different H (200 Å, 300 Å, and 400 Å) and present their corresponding focusing patterns in Figs. 4(a)–4(c), together with the 2D FFT analysis in Figs. 4(d)–4(f).

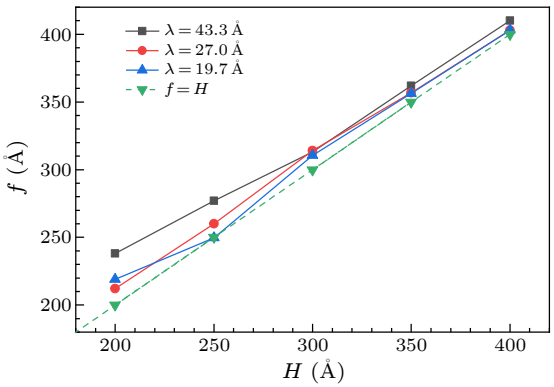

Fig. 3. The relationship between the focal length f and the height H of the structure within different phonon wavelengths. The dashed line represents the linear relationship $f = H$, which is used as a reference.

Comparing these three structures, we find that the different H values only change the location of the focusing point but do not change the mode after focusing. Moreover, a larger H makes more modes confined inside the triangular structure, resulting in a significant reduction in the energies of T1 and T2. The energy transmission coefficient after passing through these three structures are 42.67%, 10.81%, and 10.76%, respectively. It is worth noting that the time at which the focusing point emerges also changes with different H from $t = 7$ ps to $t = 9$ ps, as shown in Figs. 4(a)–4(c). These phenomena reveal that we not only can regulate the focusing position of phonon wave packets, but also can control the focusing energy intensity and focusing time by varying the height of the triangular structure.

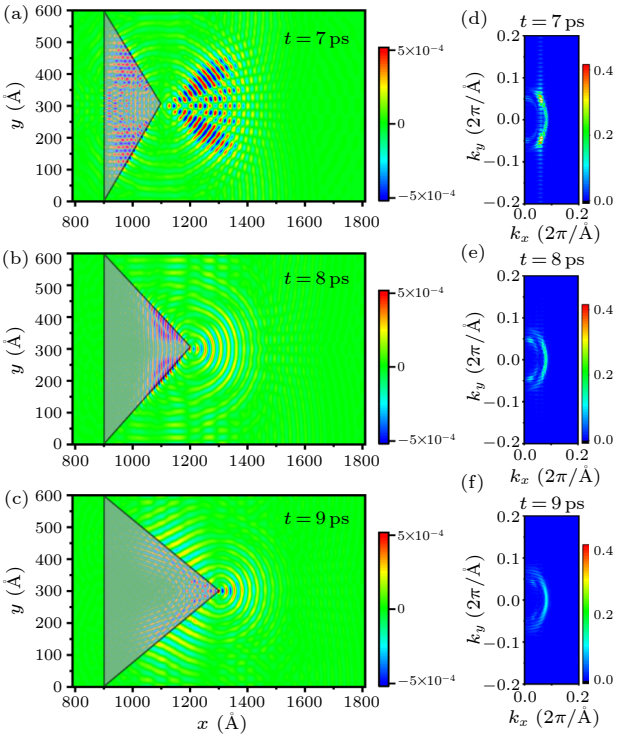

Fig. 4. (a)–(c) Distribution of atomic displacement after the phonon wave packet passes through the triangular structure with different H. The bottom edge of triangular structure is located at $x = 900$ Å. (a) Vertex is located at $x = 1100$ Å ($H = 200$ Å), (b) vertex is located at $x = 1200$ Å ($H = 300$ Å), and (c) vertex is located at $x = 1300$ Å ($H = 400$ Å). (d)–(f) The corresponding 2D FFT of the spatial displacement distribution in (a)–(c), respectively. The colorbar in 2D FFT represents the Fourier transform intensity.

One interesting question arises: What will happen if we reverse the incident direction from the vertex side of the triangular structure? Will the phonon focusing effect still hold in this case? In this regard, we finally launch wave packet on the vertex side, and simulate the wave packet propagation process in a triangular structure with $H = 200$ Å as shown in Figs. 5(a)–5(d), with their corresponding 2D FFT in the specific range ($900\,\text{Å} \leqslant x \leqslant 1600\,\text{Å}$) shown in Figs. 5(e)–5(h).

At $t = 4$ ps, the wave front of plane wave P1 that touches the hypotenuse is tilted inside the triangular structure due to the phase gradient [Fig. 5(a)], which corresponds to the rightmost two bright spots in the 2D FFT result shown in Fig. 5(e). In addition, there are still a large

number of P1 that do not touch the triangular structure, so that the original P1 mode still can be observed in 2D FFT. At $t = 5$ ps, part of the tilted mode has transported through the triangular structure [Fig. 5(b)], which appears as RT1 and RT2 modes in 2D FFT [Fig. 5(f)]. With the further propagation ($t = 6$ ps), the incident phonon wave packet passes through the triangular structure. The intensity of the tilted mode inside the triangle decreases [Fig. 5(c)], while the intensity of RT1 and RT2 increases [Fig. 5(g)]. In this case, the transmitted wave packets focus inside a certain region (from $y = 200$ Å to $y = 400$ Å) to form a large area of interference pattern in Fig. 5(c), which is completely different from the point focusing phenomenon observed in Fig. 4. This interference pattern becomes more obvious at $t = 7$ ps [Fig. 5(d)], and more modes emerge in the 2D FFT [Fig. 5(h)].

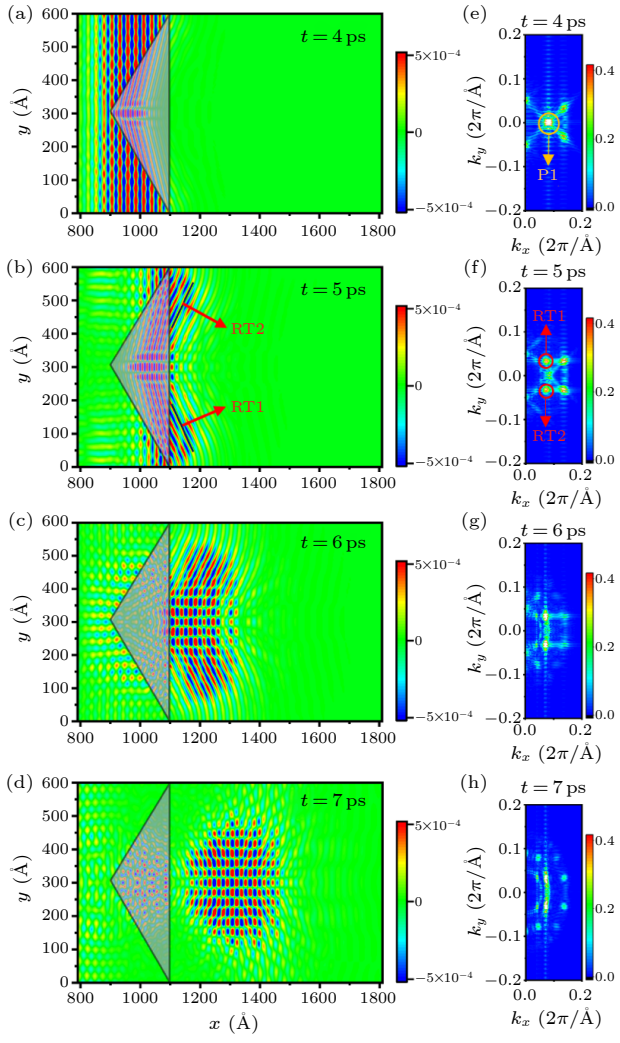

Fig. 5. (a)–(d) Displacement distribution of the phonon wave packet passing through the triangle-shaped atom-scale structure with $H = 200$ Å at different time snapshots. The vertex of the triangular structure is located at $x = 900$ Å and the bottom edge is located at $x = 1100$ Å. (e)–(h) The corresponding 2D FFT of the spatial displacement distribution in a local region ($900\,\text{Å} \leqslant x \leqslant 1600\,\text{Å}$) in (a)–(d), respectively. The colorbar in 2D FFT represents the Fourier transform intensity.

More interestingly, we find that about 88.35% of the incident energy can be transmitted through the triangular structure along this reverse incident direction (Fig. 5), which is much larger than that of 42.67% in the same structure along the positive incident direction (Fig. 2). This result also suggests a rectification effect of individual phonon wave packet [57] when passing through this triangular structure. In the positive incident direction in Fig. 2, the plane wave firstly touches the bottom edge of the triangle and most of the energy is reflected. In contrast, along the reverse incident direction in Fig. 5, the plane wave first reaches the hypotenuse of the triangle, where most of the energy is refracted into the interior of the triangular structure. Additionally, the subsequent contact with the bottom of the triangle does not have an excessive reflection effect on the tilted wave, so that the energy transmission coefficient in the reverse direction is much larger than that in the positive direction. These phenomena suggest that we can modulate the focusing pattern of phonons and energy transmission coefficient by engineering the incident direction.

In summary, we have proposed a triangle-shaped atom-scale structure to realize the phonon focusing effect in single-layer graphene. In the positive incident direction, a focusing point near the vertex of the triangular structure can be observed by controlling the phase of phonon wave packets. The detailed mode conversion process can be clearly understood from the 2D FFT analysis. We further demonstrate that the position of the focusing point and the time at which the focusing position emerges can be controlled by adjusting the height of the triangular structure. Moreover, we also find that the energy transmission coefficient decreases monotonically with the increasing height of the triangular structure. In the reverse incident direction, a completely different focusing pattern that covers a wide region is observed, and a largely enhanced energy transmission coefficient is found compared to that in the positive incident direction, suggesting that the same structure can also serve as a phononic rectifier. Our study paves the way for realizing the phonon focusing effect via atomic level structure design.

Acknowledgements. This work was supported by the National Natural Science Foundation of China (Grant Nos. 12075168 and 11890703), the Science and Technology Commission of Shanghai Municipality (Grant No. 21JC1405600), and the Fundamental Research Funds for the Central Universities (Grant No. 22120230212).

References

[1] Chen A L, Wang Y S, Wang Y F, Zhou H T, and Yuan S M 2022 *Appl. Mech. Rev.* **74** 020801
[2] Chen J, He J, Pan D, Wang X T, Yang N, Zhu J J, Yang S A, and Zhang G 2022 *Sci. China Phys. Mech. Astron.* **65** 117002
[3] Zhang Z W, Guo Y Y, Marc B, Chen J, Nomura M, and Volz S 2021 *APL Mater.* **9** 081102
[4] Gao F, Xie J L, Peng Y C, Yan B, Liu E, Peng P, Li H, Jiang J P, and Liu J J 2020 *Europhys. Lett.* **132** 38003
[5] Song X P, Chen T N, and Li R 2021 *J. Appl. Phys.* **130** 085101
[6] Cen Y, Xie J L, and Liu J J 2019 *Chin. Opt. Lett.* **17** 080501

[7] Feng Z F, Zhang X D, Wang Y Q, Li Z Y, Cheng B Y, and Zhang D Z 2005 *Phys. Rev. Lett.* **94** 247402
[8] Chen J H, Qian J, Guan Y J, Ge Y, Yuan S Q, Sun H X, Lai Y, and Liu X J 2021 *Front. Mater.* **8** 766491
[9] Ge Y, Sun H X, Yuan S Q, and Xia J P 2017 *Appl. Phys. A* **123** 328
[10] Li Y, Shen C, Xie Y B, Li J F, Wang W Q, Cummer S A, and Jing Y 2017 *Phys. Rev. Lett.* **119** 035501
[11] Song A L, Chen T N, Wang X P, and Xi Y H 2017 *Phys. Lett. A* **381** 2283
[12] Gao H, Gu Z M, Liang B, Zou X Y, Yang J, Yang J, and Cheng J C 2016 *Appl. Phys. Lett.* **108** 073501
[13] Yamamoto N and Nomura H 2021 *Jpn. J. Appl. Phys.* **60** SDDB05
[14] Zhang P, Li T C, Zhu J, Zhu X F, Yang S, Wang Y, Yin X B, and Zhang X 2014 *Nat. Commun.* **5** 4316
[15] Buckmann T, Thiel M, Kadic M, Schittny R, and Wegener M 2014 *Nat. Commun.* **5** 4130
[16] Cummer S A, Christensen J, and Alù A 2016 *Nat. Rev. Mater.* **1** 16001
[17] Han T C, Bai X, Gao D L, Thong J T L, Li B W, and Qiu C W 2014 *Phys. Rev. Lett.* **112** 054302
[18] Huang S B, Fang X S, Wang X, Assouar B, Cheng Q, and Li Y 2019 *J. Acoust. Soc. Am.* **145** 254
[19] Fleury R, Sounas D, and Alu A 2015 *Nat. Commun.* **6** 5905
[20] Mei J, Ma G C, Yang M, Yang Z Y, Wen W J, and Sheng P 2012 *Nat. Commun.* **3** 756
[21] Maldovan M 2013 *Nature* **503** 209
[22] Hu S Q, Zhang Z W, Jiang P F, Chen J, Volz S, Nomura M, and Li B W 2018 *J. Phys. Chem. Lett.* **9** 3959
[23] Yang L N, Chen J, Yang N, and Li B W 2015 *Int. J. Heat Mass Transfer* **91** 428
[24] Ma J Q, Wang S E, Wan X, Ma D K, Xiao Y, Hao Q, and Yang N 2022 *Nanoscale* **14** 17072
[25] Jiang P F, Ouyang Y L, Ren W J, Yu C Q, He J, and Chen J 2021 *APL Mater.* **9** 040703
[26] Lei M, Jiang C R, Yang F B, Wang J, and Huang J P 2023 *Int. J. Heat Mass Transfer* **207** 124033
[27] Zhang Z R, Yang F B, and Huang J P 2023 *Phys. Rev. Appl.* **19** 024009
[28] Zhang C, Ma D K, Shang M Y, Wan X, Lü J T, Guo Z L, Li B W, and Yang N 2022 *Mater. Today Phys.* **22** 100605
[29] Xu L J, Liu J R, Jin P, Xu G Q, Li J X, Ouyang X P, Li Y, Qiu C W, and Huang J P 2023 *Natl. Sci. Rev.* **10** nwac159
[30] Ji R C, Peng G L, Xu Z W, Yang N, and Hao Q 2022 *Acta Phys. Sin.* **71** 168401 (in Chinese)
[31] Jin P, Liu J R, Xu L J, Wang J, Ouyang X P, Jiang J H, and Huang J P 2023 *Proc. Natl. Acad. Sci. USA* **120** e2217068120
[32] Zhang Z W, Guo Y Y, Bescond M, Chen J, Nomura M, and Volz S 2021 *Phys. Rev. B* **103** 184307
[33] Zhang Z W, Guo Y Y, Bescond M, Chen J, Nomura M, and Volz S 2022 *Phys. Rev. Lett.* **128** 015901
[34] Zhang Z W, Guo Y Y, Bescond M, Chen J, Nomura M, and Volz S 2022 *npj Comput. Mater.* **8** 96
[35] Zong Z C, Pan D K, Deng S C, Wan X, Yang L N, Ma D K, and Yang N 2023 *Acta Phys. Sin.* **72** 034401 (in Chinese)
[36] Lu S, Ouyang Y L, Yu C Q, Jiang P F, He J, and Chen J 2021 *J. Appl. Phys.* **129** 225106
[37] Jiang P F, Hu S Q, Ouyang Y L, Ren W J, Yu C Q, Zhang Z W, and Chen J 2020 *J. Appl. Phys.* **127** 235101
[38] Pan D K, Zong Z C, and Yang N 2022 *Acta Phys. Sin.* **71** 086302 (in Chinese)
[39] Chen J, Zhang G, and Li B W 2011 *J. Chem. Phys.* **135** 104508
[40] An M, Chen D S, Ma W G, Hu S Q, and Zhang X 2021 *Int. J. Heat Mass Transfer* **178** 121630
[41] Liu B, Guo Y Y, Khvesyuk V I, Barinov A A, and Wang M R 2022 *Nano Res.* **15** 9492
[42] Hu S Q, Zhang Z W, Jiang P F, Ren W J, Yu C Q, Shiomi J, and Chen J 2019 *Nanoscale* **11** 11839
[43] Haku S, Moriya H, An H Y, Musha A, and Ando K 2021 *Phys. Rev. B* **104** 174403
[44] Chen J F, Xie J L, and Liu J J 2021 *Results Phys.* **30** 104840
[45] Gao S L, Zeng Q L, Gong M Y, Lan J, and Liu X 2022 *Micromachines* **14** 12
[46] Ulug B, Kuruoglu F, Y, Y , Erol A, Sarcan F, Sahin A, and Cicek A 2022 *J. Phys. D* **55** 225303
[47] Cheng P S, Shulumba N, and Minnich A J 2019 *Phys. Rev. B* **100** 094306
[48] Hurley D C, Wolfe J P, and McCarthy K A 1986 *Phys. Rev. B* **33** 4189
[49] Camley R E and Maradudin A A 1983 *Phys. Rev. B* **27** 1959
[50] Taylor B, Maris H J, and Elbaum C 1969 *Phys. Rev. Lett.* **23** 416
[51] Every A G 1992 *Phys. Rev. B* **45** 5270
[52] Tamura S 1983 *Phys. Rev. B* **28** 897
[53] Yang J K, Shen M, Yang Y, Evans W J, Wei Z Y, Chen W Y, Zinn A A, Chen Y F, Prasher R, Xu T T, Keblinski P, and Li D Y 2014 *Phys. Rev. Lett.* **112** 205901
[54] Schelling P K, Phillpot S R, and Keblinski P 2002 *Appl. Phys. Lett.* **80** 2484
[55] Plimpton S 1995 *J. Comput. Phys.* **117** 1
[56] Lindsay L and Broido D A 2010 *Phys. Rev. B* **81** 205441
[57] Zhang Z W, Ouyang Y L, Chen J, and Volz S 2020 *Chin. Phys. B* **29** 124402